NUMERICAL MODELING OF THE FRICTION STIR WELDING PROCESS

George Papazafeiropoulos[1], Andreas - Marios Tsainis[2]

[1]Institute of Structural Analysis and Antiseismic Research
National Technical University of Athens
Athens, GR-15780, Greece
e-mail: gpapazafeiropoulos@yahoo.gr ; web page: http://users.ntua.gr/gpapazaf/

[2]BRAT Ltd
Athens, GR-14452, Greece
e-mail: andreas_111206_@hotmail.com

Keywords: Friction Stir Welding, thermomechanical, adaptive mesh.

Abstract. *Friction Stir Welding (FSW) is a welding process which is used to join materials, usually metals or thermoplastics, together. The advantages of FSW over conventional fusion welding methods involve the elimination of solidification cracking, liquation cracking and porosity, and the improved mechanical properties of the weld. Despite its simple and successful application in aerospace, shipbuilding, aircraft, and automobile industries, the inherent nature of the process is not yet fully understood. In order to design and/or optimize the FSW process effectively, reliable numerical models have to be developed, which will simulate complex thermo-mechanical response and friction phenomena and will verify the experimental data. In this study the plunging phase of the FSW process is studied numerically using the finite element method. A three-dimensional fully coupled thermal-stress finite element model has been developed in ABAQUS/Explicit, in which the arbitrary Lagrangian Eulerian (ALE) formulation is used to simulate severe element distortion using an adaptive mesh scheme. The simulation results include temperature profiles, force and moment of the tool, as well as plastic and frictional dissipation energy.*

1 INTRODUCTION

Friction Stir Welding, a method of solid state joining process, was invented by W. Thomas and his colleagues of The Welding Institute (TWI), UK, in 1991. In this process, using a rotational probe of a material harder than the workpieces to be welded, the workpiece material is plasticized and an effective transportation mechanism is provided for the plasticized material to join the workpieces together. The process consists of three phases: plunging, dwelling, stirring, and retraction. It starts with spinning the tool and slowly vertically plunging it into the seam line of the two rigidly clamped parts on a backing plate, until the shoulder contacts the top surface of workpiece to further increase the volume of the deformed material (plunging period). This period is followed by the dwelling period in which the tool is held at a constant position relative to the workpiece but still rotating, until the temperature reaches a certain value. After that, the tool begins a forward traverse motion along a predetermined path, creating a fine grained recrystallized microstructure behind it (stirring period). Finally, in the retraction period, the tool draws away from the workpieces being welded.

This process has been widely used in many industries such as space, aircraft, marine, transport and food processing. Friction stir welding has been applied to metals with moderate melting points. Initially, FSW was applied primarily to aluminum alloys, which could be easily welded due to their relatively low softening temperature. Other relatively soft metals, such as copper, lead, zinc, and magnesium, have also been welded using this method. The last can be applied also for dissimilar welds, where different materials are being welded. The main advantages of FSW are low distortion, high quality, lower residual stresses, fewer weld defects and low cost joints.

Despite the simplicity of the FSW method, the processes involved in it are not yet completely understood. Modeling heat generation and heat transfer processes within FSW requires understanding several other physical processes: material flow around the welding tool, contact pressure inflicted by the welding tool, friction coefficient, wear, change of thermo-mechanical properties and heat transfer coefficients, etc. Although the process has very few parameters that can be controlled, the way they affect the final weld is not clear yet.

2 LITERATURE REVIEW

Since its development FSW has been widely analyzed, both experimentally and using analytical and/or numerical models. The first models of the process addressed mainly the thermal response.

2.1 Analytical Models for Heat Generation

Various analytical models for the simulation of the thermal processes during FSW have been proposed. The simplest model involves the consideration of the local heat generation, which is given by:

$$q = \tau \omega r \tag{1}$$

where τ is the shear stress located at a segment of the contact interface between the tool and the shear layer, ω is the angular velocity and r is the distance of the surface segment from the tool axis. Based on the above relation, various expressions for the heat generated during FSW can be derived analytically. The local heat generation is one of the most important parameters when developing a thermal model of FSW. In [1], an analytical expression for estimating heat generation for a complex tool shape is proposed. Its distribution can be prescribed as a thermal boundary condition in a numerical model or used in an analytical model to estimate the total heat generation. However the above model has several limitations (e.g. it cannot be used directly to investigate the effect of the welding speed).

2.2 Numerical Models

In order for the FS welds to be sound, not only the various parameters involved must take values within certain limits, but also they have to be properly combined. The optimum parameter combinations for FS welds have been obtained almost exclusively through experimental data, due to the fact that the phenomena which take place during the FSW process are not yet completely understood. Consequently, there is a strong need for realistic numerical simulations, which help to better understand and observe the effect of the various parameters of the problem on the resulting temperature field or material flow, results which cannot be always measured directly in an experiment. Concerning Al2023-T4 welds, results are presented in the studies described in the following paragraphs.

One of the first studies to address the mechanical interaction between the tool and the welded panels in FSW is presented in [2]. Sequentially coupled thermo-mechanical FE analyses were conducted using ABAQUS/Standard, i.e. the temperature field was generated first and then read by the mechanical model. The temperature results from the model were verified by experiments, which proved that the heat source model was considered to be sufficiently accurate.

Lockwood and Reynolds in [3] have studied the local and global mechanical responses of friction stir welding experimentally and numerically. Two-dimensional FE modeling of welded thin plates of aluminum alloy 2024-T351 gave results which agree with experimental data, revealing nearly plane stress conditions in the plates. The results have been corroborated by a three-dimensional FE model.

Schmidt et al. in [1] proposed a more general analytical model for heat generation based on various contact conditions at the tool/matrix interface, namely sliding, sticking, and partial sticking condition. They concluded that the sticking condition prevailed at the tool/matrix interface of Al2024-T3 alloy, based on experimental data on heat generation rate and plunge force.

Schmidt & Hattel in [4] have adopted a fully coupled thermo-mechanical dynamic analysis model in ABAQUS/Explicit, using the Arbitrary Lagrangian–Eulerian (ALE) formulation and the Johnson–Cook material law. The model accounts for the compressibility by including the elastic response of the aluminum matrix. The contact forces are modeled by Coulomb's Law of friction. It was shown that heat generation is primarily caused by plastic dissipation since the sticking condition is present at the most part of the contact interface.

Zhang et al. in [5] used a fully coupled thermo-mechanical finite element model for different thicknesses of the welded plates. It was estimated that 54% of the total input energy is transferred to the welding plates and 85.3% can be converted to frictional heat.

In [6] a simple three-dimensional thermo-mechanical model for FSW is developed based on a combination of fluid mechanics numerical and analytical velocity fields. In order to compute the temperature field during welding the velocity fields are introduced in a steady state thermal calculation. In addition, they allow partial sliding between the shoulder and the workpiece. The amount of sliding appears to be significantly influenced by the welding conditions and physical interpretations are proposed for its evolution.

Li et al. in [7] studied several welding methods numerically, including FSW, using the ABAQUS software. A 3D model using fully sticking conditions for the tool-workpiece interface was developed to lead to better simulation results with the help of the ALE adaptive mesh controls option in ABAQUS/Explicit package and the map solution technique in the ABAQUS/Standard package combined with the HYPERWORKS software. The experiments that are performed validate the feasibility and accuracy of the developed models.

Sanjeev et al. in [8] in their paper aims at discussing the effect of the coefficient of friction on simulation outputs. In addition, the modification required in friction model to get realistic results from Friction Stir Welding simulations using ABAQUS software is highlighted. It was found that a coefficient of friction equal to 1.0 has to be considered with sticking condition while using Coulomb law of friction in modeling of FSW and its variants. Also, it was noted that the models with no slip condition and Johnson-Cook material model are capable of predicting correct output parameters of the FWS process.

3 NUMERICAL MODELING

3.1 Introduction

The thermomechanical problem of the FSW process is modeled numerically using the finite element code Abaqus 6.13. In the model developed, only the plunging phase is considered. An explicit integration procedure was implemented by using Abaqus/Explicit, since it allows for a solution which is less computationally expensive and less susceptible to errors (e.g. due to excessive element distortion, etc.).

3.2 Geometry

The model is comprised of a cylindrical welding tool with unthreaded pin and shoulder, the plates to be welded (simulated in this study in a simplified way as a single part) and the backing plate, which serves to support the tool and the welded plate, as shown in Figure 1. The welded workpiece and the backing plate have dimensions 100 mm length and 50 mm width, while the thickness of the workpiece and the backing plate is 3mm and 30mm respectively. The welding tool has a pin with diameter equal to 6mm, whereas its shoulder has diameter 18mm. The height of the tool is 11mm, of which 2mm is the height of the pin.

The workpiece is assumed to be made of a deformable material (Al2024-T3) that has displacement and temperature degrees of freedom. In order to avoid excessive element distortion due to large values of aspect ratio, the last is kept equal to unity for all elements of the workpiece, the mesh of which is unbiased along all its dimensions. The edge length of each element at the workpiece is equal to 1mm. The backing plate and the tool have coarser meshes, since no significant deformation appears to them. The mesh of the model has 21804 nodes and 15896 elements. The workpiece and the backing plate are discretized with C3D8RT elements, whereas the tool is discretized with C3D6RT elements, due to its curved geometry. These element types have a coupled temperature – displacement formulation, i.e. they have 8-node tri-linear displacement and temperature degrees of freedom and they use reduced integration with hourglass control. The tool is modeled as a rigid body, since its deformation is negligible compared to that of the welded workpiece plate. However, its thermal response is maintained exactly as if it were deformable. In Figure 1 the undeformed configuration of the model used in this study is shown.

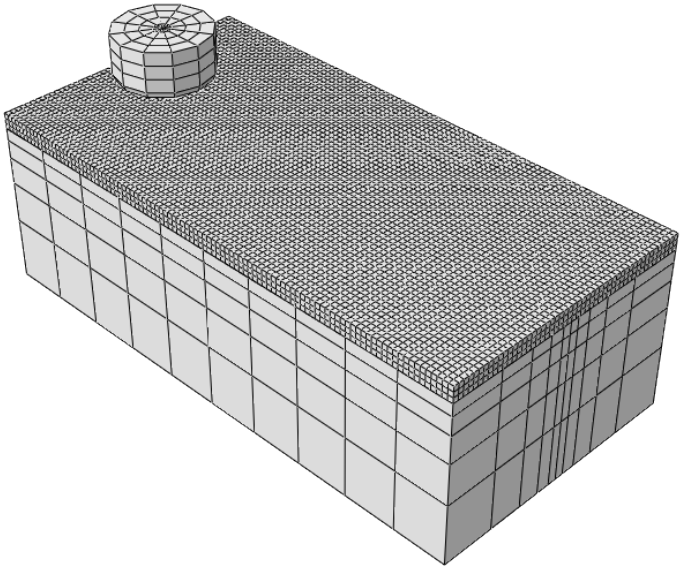

Figure 1. Reference configuration of the model used for the numerical simulations.

3.3 Welding Parameters

The parameters that can be controlled during the FSW process are the rotational speed, the plunge rate and the weld rate of the tool. However, since in this study the welding phase is not considered, only the two first

parameters are taken into account. These parameters are prescribed as angular velocity and vertical displacement at the reference point of the tool respectively.

3.4 Assumptions

FSW is a process inherently complicated; therefore, to obtain models which are both computationally affordable and realistic, a number of simplifying assumptions have to be made. The simplifications made in this study are the following:

a) The workpiece and the tool are assumed to have frictional sliding contact described by Coulomb's friction law.

b) The tool is considered to be a rigid body that has translational and rotational degrees of freedom, with a reference point which describes only its mechanical response. This reference point controls the rigid body motion of the tool. The temperature field inside it is independent of the reference point and can have any acceptable distribution.

c) The initial temperature for the workpiece, tool and backing plate is assumed to be 25^{o}C and is defined as a predefined field at the initial step of the analysis.

d) It is assumed that all the dissipated energy caused by friction is transformed into heat. At the tool – workpiece interface, 60% of the above converted heat is distributed to the workpiece.

3.5 Boundary Conditions

Since a coupled thermomechanical model is considered in this study, the boundary conditions can be either mechanical or thermal. Boundary conditions of both types are imposed to the model. Regarding the mechanical boundary conditions, the bottom and vertical surfaces of the backing plate are constrained at all directions (x, y and z). The same holds for the vertical surfaces on the perimeter of the workpiece. The reference point of the tool is constrained along both horizontal directions (x and z) and a vertical downward displacement is imposed to it with ramp amplitude (i.e. a constant velocity equal to u_y). As far as the rotational degrees of freedom are concerned, rotations with respect to x and z axes are fixed, whereas a constant angular velocity ω is specified along y direction.

Regarding the thermal boundary conditions, heat convection coefficients are specified for all the surfaces of the model which are exposed to the air. The ambient temperature T_{inf} is considered to be 25^{o}C (roughly 298 K). The heat convection coefficient for each surface is calculated as follows:

$$h = \frac{Nu_L \cdot k}{L} \tag{1}$$

where Nu_L is the Nusselt number given by:

$$Nu_L = 0.54 \cdot Ra_L^{1/4} \tag{2}$$

The Rayleigh number Ra_L is calculated by the relation:

$$Ra_L = Pr \cdot Gr_L \tag{3}$$

where P_r and Gr_L are the Prandtl and Grashof numbers respectively, with the latter given by:

$$Gr_L = \frac{10 \cdot b \cdot (T_s - T_{inf}) \cdot L^3}{v^2} \tag{4}$$

In the relation (4) b is the expansion coefficient of the air, T_s is the temperature at the surface under consideration, L is the characteristic length, given by either the surface-to-perimeter ratio or the volume-to-surface ratio, and v is the kinematic viscosity of the air. The heat convection coefficient is specified as a function of the surface temperature in tabular form.

3.6 Contact Interfaces

Similar to the nature of the boundary conditions imposed to the model, the surfaces of the various parts of the model which come in contact can interact both mechanically and thermally. As far as the mechanical response is concerned, at the tool-workpiece interface Coulomb friction with coefficient μ equal to 0.3 and hard contact with

separation are specified. The workpiece-backing plate interface is considered to be rough with hard contact without separation after contact. Finite sliding formulation was used for both interfaces. For the workpiece-backing plate interface the penalty contact formulation is used, whereas for the tool-workpiece interface the kinematic contact formulation is used.

Regarding thermal response, at the tool-workpiece interface a pressure-dependent thermal gap conductance is specified, ranging approximately from 500 to 7000 W/m^2K. All the dissipated energy caused by friction is assumed to be converted to heat, approximately 60% of which is distributed to the workpiece. At the workpiece-backing plate interface a pressure-dependent thermal gap conductance is specified, ranging approximately from 1400 to 8500 W/m^2K. All the dissipated energy caused by friction is assumed to be converted to heat, approximately 57.1% of which is distributed to the workpiece.

3.7 Material Model and Properties

Aluminum alloy Al2024-T3 was chosen as the workpiece material. Its chemical composition and other properties are shown in [9]. To simulate its behavior in the analysis, a strain hardening, strain rate hardening and temperature softening material law is used, using the elastic-plastic Johnson-Cook material model [10], which is given by:

$$\sigma_y = \left(A + B\varepsilon^n\right)\left[1 + C\ln\left(1 + \frac{\dot{\varepsilon}}{\dot{\varepsilon}_0}\right)\right]\left[1 - \left(\frac{T - T_{inf}}{T_{melt} - T_{inf}}\right)^m\right] \quad (5)$$

where σ_y is the yield stress, ε is the effective plastic strain, $\dot{\varepsilon}$ is the effective plastic strain rate, $\dot{\varepsilon}_0$ is the reference strain rate (typically 1.0 s^{-1}). A, B, n, C, T_{melt}, and m are material constants, which are listed in Table 1. Apart from these constants, all the remaining material properties are temperature-dependent. T_{inf} is the ambient temperature, which is considered to be 25° C in this study.

The tool and the backing plate are modeled as linear elastic, and they are given the material properties of Cr-V-Mo steel (56NiCrMoV7) and steel 42CrMo4, respectively. The variations of the mechanical and thermal properties of these two materials with temperature are shown in Tables 2 and 3 respectively. In case a property is not explicitly defined in the tables, linear interpolation between neighboring values is performed.

3.8 Finite Element Techniques

In order to make the analyses faster and more efficient, two auxiliary options are used. Firstly, the Arbitrary Lagrangian – Eulerian (ALE) adaptive meshing is used in the model developed in this study. Generally this provides control of the mesh distortion if large deformation occurs. The analyses performed in this study involve geometric nonlinearities and therefore the model is expected to undergo large deformations. The term ALE implies that the analysis approach lies between Lagrangian analysis, where the node motion is identical to the material motion, and Eulerian analysis, where the nodes remain fixed in space and the material flows through the elements. Since the tool is modeled as a rigid body and the backing plate is not expected to exhibit large deformations, adaptive meshing is used only for the workpiece. The adaptive meshing is set to be made after each 5 increments and each adaptive meshing includes 4 mesh sweeps for optimizing the node positions.

A	265 MPa
B	426 MPa
n	0.34
C	0.015
m	1.00
T_{melt}	502 °C
Modulus of elasticity	73.1 GPa
Poisson ratio	0.33
Thermal expansion	2.28×10^{-5} K^{-1}
Specific Heat Capacity	870 J/(Kg*K)
Thermal Conductivity	120 W/(m*K)
Density	2770 Kg/m^3

Table 1 : Properties of workpiece material (Al2024-T3)

	Modulus of elasticity	Poisson ratio	Thermal expansion	Specific heat capacity	Thermal conductivity	Density
[°C]	[GPa]	[-]	[K^{-1}]	[J/(Kg*K)]	[W/(m*K)]	[Kg/m^3]
20	215	0.3		460	36	7800
100			12.2×10^{-6}			
200			13×10^{-6}			
300			13.3×10^{-6}			
350					38	
400	198	0.3	13.7×10^{-6}			
500	176	0.3	14.2×10^{-6}	550		7640
600	165	0.3	14.4×10^{-6}	590		7600
700					35	

Table 2 : Properties of tool material (55NiCrMoV7) and their variation with temperature

	Modulus of elasticity	Poisson ratio	Thermal expansion	Specific heat capacity	Thermal conductivity	Density
[°C]	[GPa]	[-]	[K^{-1}]	[J/(Kg*K)]	[W/(m*K)]	[Kg/m^3]
-100	217	0.3	10.5×10^{-6}	423		
0	213	0.3	11.4×10^{-6}	456		7850
20	230	0.3	11.5×10^{-6}	461	45.1	7850
100	207	0.3	12.1×10^{-6}	479	45.1	7850
200	199	0.3	12.7×10^{-6}	499	44.1	7850
300	192	0.3	13.2×10^{-6}	517	41.9	7850
400	184	0.3	13.6×10^{-6}	536	39.4	7850
500	175	0.3	14×10^{-6}	558	36.9	7850
600	164	0.3	14.4×10^{-6}	587	34.4	7850

Table 3 : Properties of backing plate material (42CrMo4) and their variation with temperature

Additionally, mass scaling was defined in the analysis steps. In Abaqus/Explicit, the explicit central difference method is used to integrate the equations in time, and thus the mass matrix used in the equilibrium equations plays a crucial role in both computational efficiency and accuracy. The FSW process has a dynamic nature, given that the workpiece material has rate-dependent properties, so the natural time scale is important. It was found from the results of some initial trial runs that the pin contains a few very small elements due to its geometry, which have stable time increments substantially lower than the average, leading to a very small time increment for the whole model. To fix this, an element stable time increment was specified for the whole model, equal to 0.001 sec, at the beginning of the step (i.e. fixed mass scaling). The elements being significantly affected by the mass scaling are very few; the effect on the overall behavior of the model is negligible.

4 RESULTS

Four typical FSW cases were analyzed in this study, two of which are nearly identical to the cases presented in [9]. The four cases result from combinations of two typical plunging velocities u_y and two typical rotation speeds ω. For u_y two values were considered: 6mm/min and 4 mm/min and for ω two values were considered: 400rpm and 447rpm. The relevant results are shown in the following sections.

4.1 Thermal Profiles

The distributions of the temperature along the system are shown in Figure 2. It is seen that for u_y=6mm/min and ω=400rpm the workpiece has maximum temperature roughly 435^{o}C, for u_y=6mm/min and ω=447rpm the workpiece has maximum temperature roughly 415^{o}C, for u_y=4mm/min and ω=400rpm the workpiece has

maximum temperature roughly 461^{o}C and for u_y=4mm/min and ω=447rpm the workpiece has maximum temperature around 502^{o}C. In all cases the maximum temperature of the welded material occurs under the shoulder of the tool, near the pin. The two first of the aforementioned cases compare well to the results presented in [9]. Generally, it is observed that the workpiece experiences higher temperatures for lower plunging speeds and conversely. The tool seems to have higher temperatures than the underlying workpiece in general, for all cases examined. Concerning the temperature profile in the backing plate, the temperature shows less pronounced variation compared to the whole model, remaining closer to the ambient temperature (25^{o}C).

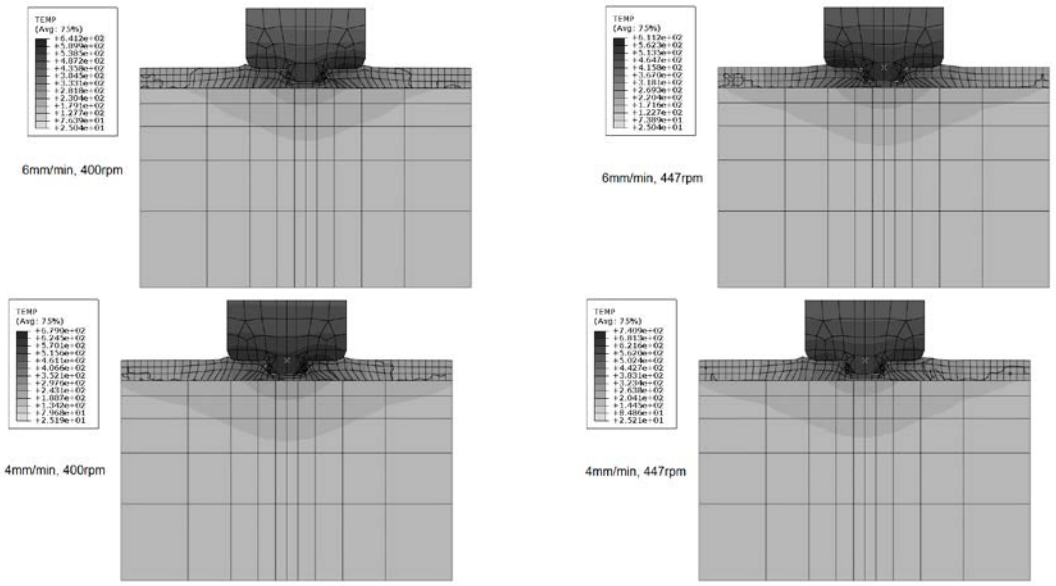

Figure 2. Thermal profiles of the four FSW cases studied.

4.2 Plunging Force

In Figure 3 the plunging force required for the FSW process versus time is plotted for the four cases considered in this study. It is observed that the case with ω=447rpm and u_y=6mm/min requires the largest plunging force of all cases. On the other hand, the case with ω=400rpm and u_y=4mm/min requires the lowest force. These results compare well with the plunging force presented in [9], where it was calculated to be equal to approximately 14kN. Furthermore, it is apparent that after an initial increase, the plunging force almost stabilizes for the time period of the plunging phase, a trend which is noted in all FSW cases considered. Finally, as it is expected, the plunging force increases with the plunging speed.

4.3 Torque

In Figure 4 the torque required for the FSW process versus time is plotted for the four cases considered in this study. The four cases examined show similar trends, and the variations from case to case are relatively small. It is seen that after a time period of approximately 15 sec, the torque seems to increase. This is attributed to the fact that at that time moment the shoulder of the tool comes in contact with the workpiece, which due to the plunging of the pin, has moved upwards as a result of its deformation. Then, frictional forces are present in a larger radius from the tool axis than those present at the pin-workpiece interface, and this results in the torque increase noted in Figure 4. Moreover, it is obvious that the torque almost stabilizes for a relatively large time period during the FSW process and always before the shoulder of the tool comes in contact with the welded material.

4.4 Plastic to frictional energy ratio

An essential aspect of the FSW process is the way the input energy from the tool is dissipated during its conversion to heat. The proportionality each kind of heat source depends on the phase of the process and, primarily on the temperature of the workpiece material. In Figure 5 the ratio of the energy dissipated by rate-independent and rate-dependent plastic deformation to the energy dissipated through frictional effects is shown. It is obvious that the ratio increases continuously during the process, meaning that the energy due to plastic deformation increases with respect to the energy due to frictional effects. The proportion becomes higher for welds in which the plunging speed is higher. In addition, for constant plunging speed, the weld with the higher

angular velocity seems to have the lower proportion of the energy due to plastic deformation.

4.5 Heat generation

The heat generated during the FSW process has been calculated for the cases considered in this study. This heat propagates either through conduction in the various parts and interfaces of the model, or through convection to the environment, and is calculated by subtraction of the total internal strain energy of the model from the external work performed by the tool. In Figure 6 the total heat generated is plotted versus time. It is noted that the heat generated increases almost proportionally with time during the initial phase of the plunging process (i.e. for the period during which the shoulder of the tool has not come in contact with the workpiece). After the contact occurs, the slope of the curve increases, which means that the rate of heat production gets larger. Similarly to the interpretation of the increasing torque during this time period, this is explained by the fact that the contact area of the shoulder has larger mean radius from the tool axis than that of the pin.

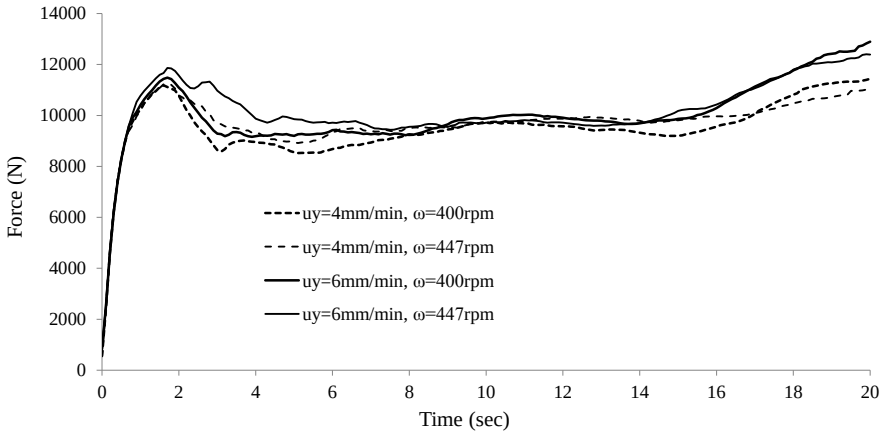

Figure 3. Plunging force during FSW process versus time for the four cases considered in this study.

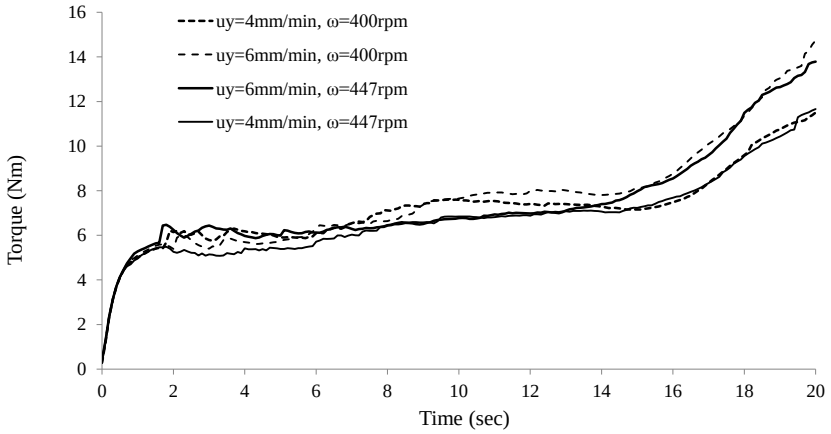

Figure 4. Torque during FSW process versus time for the four cases considered in this study.

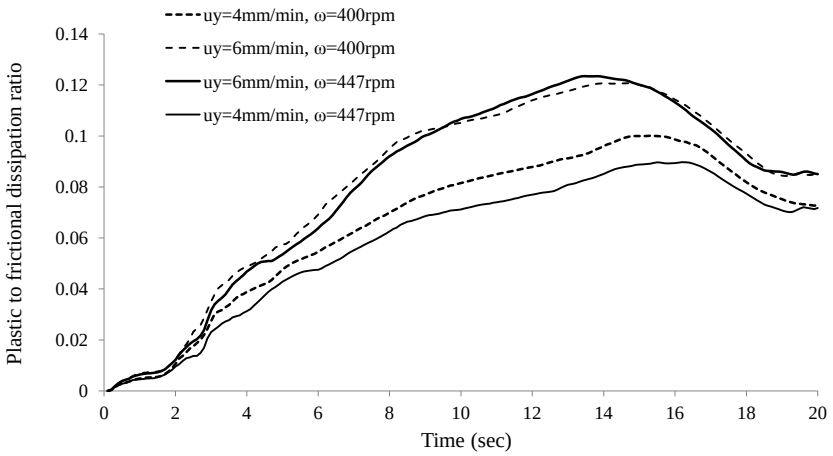

Figure 5. Ratio of energy coming from plastic deformation to the energy coming from friction during FSW process versus time for the four cases considered in this study.

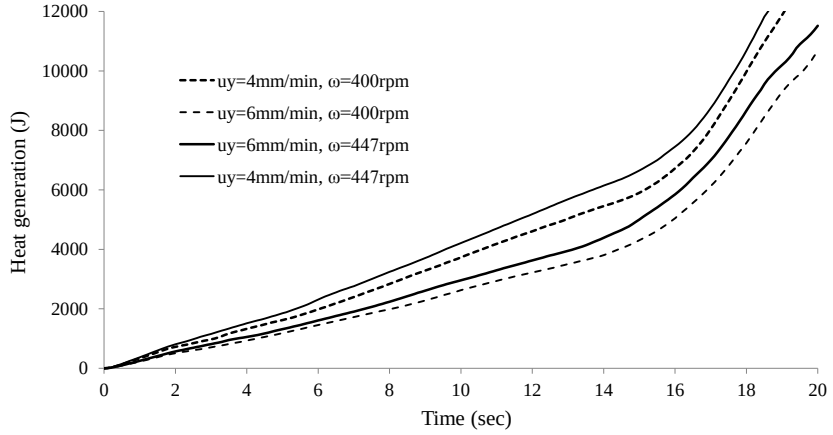

Figure 6. Total heat generation during FSW process versus time for the four cases considered in this study.

5 CONCLUSIONS

In this study four indicative FSW processes are analyzed. It is shown that the plunging and rotation speeds affect substantially the thermal profile of the system, the type of energy dissipation, and the required force and torque. Increased rotating speed combined with low plunging speed lead to increased heat generation during the process. Furthermore, it is shown that increased plunging speed leads to higher energy dissipated through plastic deformation in proportion to the energy originating from frictional effects. Explicit modeling of the backing plate and the tool allow for the more accurate calculation of the temperature distribution in the system. Thanks to this fact, it was observed that relatively low temperatures develop in the backing plate and that the highest temperature in the system occurs in the tool, near its interface to the welded material.

REFERENCES

[1] Schmidt, H., Hattel, J., Wert, J. (2004), "An analytical model for the heat generation in friction stir welding," *Modelling Simul. Mater. Sci. Eng*., Vol.12, pp.143–157.

[2] Shi, Q., Dickerson, T., Shercliff, H.R. (2003), "Thermo-mechanical FE modelling of friction stir welding of Al-2024 including tool loads", 4th International Symposium on Friction Stir Welding, Park City, Utah, USA, 14-16 May 2003.

[3] Lockwood, W.D., and Reynolds, A.P. (2003), "Simulation of the global response of a friction stir weld using local constitutive behaviour," *Materials Science and Engineering*, A339, pp.35-42.

[4] Schmidt, H., Hattel, J. (2005), "A Local Model for the Thermo-mechanical Conditions in Friction Stir Welding," *Modelling and Simulation in Mat. Science and Eng.*, Vol.13, pp.77-93.

[5] Zhang, Z., Chen, J.T., Zhang, Z.W., Zhang, H.W. (2011), "Coupled thermo-mechanical model based comparison of friction stir welding processes of AA2024-T3 in different thicknesses," *J Mater Sci*, Vol.46, pp.5815–5821.

[6] Jacquin, D., Meester, B., Simar, A., Deloison, D., Montheillet, F., Desrayaud, C. (2011), "A simple Eulerian thermomechanical modeling of friction stir welding," *Journal of Materials Processing Technology*, Vol.211, pp.57–65.

[7] Li, W., Shi, S., Wang, F., Zhang, Z., Ma, T. and Li, J., (2012), "Numerical simulation of friction welding processes based on ABAQUS environment" *Journal of Engineering Science and Technology Review*, Vol. 5, pp. 10-19.

[8] Sanjeev, N.K., Vinayak, M. and Suresh Hebbar H. (2014), "Effect of Coefficient of Friction in Finite Element Modeling of Friction Stir Welding and its Importance in Manufacturing Process Modelling Applications" Int. Journal of Applied Sciences and Engineering Research, Vol. 03, pp. 755-762.

[9] Veljic, D.M., Sedmak, A.S, Rakin, M.P., Bajic, N.S., Medjo, B.I., Bajic, D.R., and Grabulov, V.K. (2014), "Experimental and numerical thermo – mechanical analysis of friction stir welding of high – strength alluminium alloy" Thermal Science, Vol. 18, pp. S29-S38.

[10] Johnson, G. R., Cook, W. H. (1983), "A Constitutive Model and Data for Metals Subjected to Large Strains, High Strain Rates and High Temperatures," *Proceedings of the 7th International Symposium on Ballistics*, Hague, Netherlands, pp. 541-547.